AGU ADVANCING EARTH AND SPACE SCIENCE

Iron Depletion in the Deep Chlorophyll Maximum: Mesoscale Eddies as Natural Iron Fertilization Experiments

Nicholas J. Hawco[1,2] , Benedetto Barone[2] , Matthew J. Church[3] ,
Lydia Babcock-Adams[4] , Daniel J. Repeta[4] , Emma K. Wear[3] , Rhea K. Foreman[2] ,
Karin M. Björkman[2], Shavonna Bent[4], Benjamin A. S. Van Mooy[4], Uri Sheyn[2],
Edward F. DeLong[2], Marianne Acker[4], Rachel L. Kelly[1] , Alexa Nelson[2], John Ranieri[3],
Tara M. Clemente[2], David M. Karl[2] , and Seth G. John[1]

[1]Department of Earth Sciences, University of Southern California, Los Angeles, CA, USA, [2]Department of Oceanography, University of Hawai'i at Mānoa, Honolulu, HI, USA, [3]Flathead Lake Biological Station, University of Montana, Polson, MT, USA, [4]Woods Hole Oceanographic Institution, Woods Hole, MA, USA

Abstract In stratified oligotrophic waters, phytoplankton communities forming the deep chlorophyll maximum (DCM) are isolated from atmospheric iron sources above and remineralized iron sources below. Reduced supply leads to a minimum in dissolved iron (dFe) near 100 m, but it is unclear if iron limits growth at the DCM. Here, we propose that natural iron addition events occur regularly with the passage of mesoscale eddies, which alter the supply of dFe and other nutrients relative to the availability of light, and can be used to test for iron limitation at the DCM. This framework is applied to two eddies sampled in the North Pacific Subtropical Gyre. Observations in an anticyclonic eddy center indicated downwelling of iron-rich surface waters, leading to increased dFe at the DCM but no increase in productivity. In contrast, uplift of isopycnals within a cyclonic eddy center increased supply of both nitrate and dFe to the DCM, and led to dominance of picoeukaryotic phytoplankton. Iron addition experiments did not increase productivity in either eddy, but significant enhancement of leucine incorporation in the light was observed in the cyclonic eddy, a potential indicator of iron stress among *Prochlorococcus*. Rapid cycling of siderophores and low dFe:nitrate uptake ratios also indicate that a portion of the microbial community was stressed by low iron. However, near-complete nitrate drawdown in this eddy, which represents an extreme case in nutrient supply compared to nearby Hawaii Ocean Time-series observations, suggests that recycling of dFe in oligotrophic ecosystems is sufficient to avoid iron limitation in the DCM under typical conditions.

1. Introduction

Approximately 30% of the ocean's surface is subject to phytoplankton iron (Fe) limitation, especially in the Equatorial Pacific and Southern Oceans where upwelling provides a large flux of nitrate (NO_3^-) and other nutrients (Moore et al., 2001, 2013). Elsewhere, stratification of the upper ocean leads to depletion of NO_3^-, ammonia, and other bioavailable forms of nitrogen. In stratified oligotrophic gyres, shallow mixed layers also act to concentrate Fe deposited at the ocean's surface by atmospheric sources (Boyle et al., 2005; Sedwick et al., 2005). The large flux of Fe relative to NO_3^- in these ecosystems results in nitrogen limitation of photosynthesis and selects for phytoplankton like the cyanobacterium *Prochlorococcus* (Ward et al., 2013; Wu et al., 2000), whose small size allows them to outcompete other phytoplankton for recycled nitrogen species found at nanomolar concentrations (Morel et al., 1991).

However, the same stratification that leads to Fe-rich conditions in the surface ocean can also impede Fe supply to the subsurface. Shallow mixed layers ensure that Fe derived from dust deposition does not reach the entirety of the euphotic zone, which can extend below 100 m in subtropical gyres. Stratification also limits the supply of regenerated Fe from below the euphotic zone. Indeed, a common feature of dFe profiles within subtropical gyres is a concentration minimum between 75 and 150 m (Bruland et al., 1994; Fitzsimmons et al., 2015; Sedwick et al., 2005). This subsurface dFe minimum often coincides with the deep chlorophyll maximum (DCM), a unique habitat where low irradiance drives phytoplankton photo-acclimation, increasing chlorophyll per cell to improve photosynthetic light capture (Letelier et al., 2004). Theoretical arguments suggest the increases in chlorophyll per cell should be matched by an equivalent increase in the number of Fe-bearing photosynthetic reaction

Visualization: Nicholas J. Hawco, Benedetto Barone, Lydia Babcock-Adams, Emma K. Wear
Writing – original draft: Nicholas J. Hawco, Seth G. John
Writing – review & editing: Nicholas J. Hawco, Benedetto Barone, Matthew J. Church, Lydia Babcock-Adams, Daniel J. Repeta, Emma K. Wear, Rhea K. Foreman, Karin M. Björkman, Shavonna Bent, Benjamin A. S. Van Mooy, Uri Sheyn, Edward F. DeLong, David M. Karl, Seth G. John

centers, increasing cellular Fe requirements substantially if chlorophyll antennae sizes cannot be increased (Raven, 1990; Strzepek et al., 2019; Sunda & Huntsman, 1997).

The combination of low Fe supply and high demand allows dFe in the DCM of the North Pacific Subtropical Gyre to fall below 100 pM, similar to dFe measured in the Fe-limited Equatorial Pacific and Southern Ocean (Coale et al., 1996; Martin et al., 1990). It is unclear if the growth of phytoplankton in the DCM is Fe-limited at these concentrations. Classical explanations of the DCM emphasize the optimization of opposing gradients in light and nutrient flux without invoking Fe specifically (Cullen, 2015; Letelier et al., 2004). This balance is borne out in the seasonal cycle at Station ALOHA, a site that is broadly representative of the North Pacific Subtropical Gyre (Karl et al., 2021). Increasing light intensity from winter to summer allows the DCM to deepen into the nutricline, which enhances NO_3^- uptake and increases phytoplankton biomass (Letelier et al., 2004). In both seasons, the DCM is positioned at a similar light flux: roughly 0.5 mol photon m^{-2} day^{-1}, a threshold that has also been identified in other oligotrophic regions (Mignot et al., 2014), implying a fundamental control by light. However, recent experiments in the California Current Ecosystem have shown that eukaryotic phytoplankton in the DCM, especially diatoms, respond more strongly to concurrent increases in both Fe and light, compared to increases in light alone, suggesting that Fe limitation may influence productivity in that region (Hogle et al., 2018; Hopkinson & Barbeau, 2008). From this perspective, it may be significant that the seasonal deepening of the DCM at Station ALOHA coincides with a springtime increase in Fe supply from Asian dust (Boyle et al., 2005).

Definitive evidence of Fe limitation in surface waters ultimately demanded the upscaling of Fe addition experiments from liter-sized bottles to the ecosystem scale via *in situ* fertilization experiments (Boyd et al., 2007), and from parallel studies of natural iron fertilization events: coastal Fe input from islands (Blain et al., 2007; Martin et al., 1994; Pollard et al., 2009), or atmospheric deposition from dust storms (Bishop et al., 2002) and volcanic eruptions (Achterberg et al., 2013; Hamme et al., 2010). At present, there are significant logistical (not to mention ethical [Strong et al., 2009]) challenges facing would-be Fe fertilization experiments in the lower euphotic zone: the DCM cannot be observed by satellite and is out of reach of most underway sampling systems. Natural Fe fertilization events to the oligotrophic DCM (if they can be observed) represent an alternate approach.

Here, we show how perturbations to light, nutrient and iron supply caused by mesoscale eddy activity can be used to examine the vulnerability of phytoplankton in the DCM to iron limitation. This scheme is then applied to two adjacent eddies, a cyclone and an anticyclone, observed in the North Pacific Subtropical Gyre during Summer 2017. Along with several recent studies (Browning et al., 2021; Ellwood et al., 2020; Sedwick et al., 2020), our measurements also show that local Fe cycling is strongly perturbed by mesoscale eddies.

2. Methods

2.1. Expedition Summary

Sampling and experiments were conducted on the R/V *Kilo Moana* as part of the MESO-SCOPE expedition (26 June to 15 July 2017) in the North Pacific Subtropical Gyre. Satellite altimetry was accessed from the Copernicus Marine Environmental Monitoring Service and processed as described by Barone et al. (2019) to remove the seasonal cycle and interannual trend. The centers of the two mesoscale eddies sampled in this study were identified as maxima and minima of corrected sea level anomaly (SLA_{corr}): a cyclonic eddy centered at 24.9°N, 158.7°W, and an anticyclonic eddy centered at 26.4°N, 158.0°W. An initial survey of the subsurface density structure across the upper water column was performed with an underway CTD (Teledyne), followed by hydrographic sampling for metals and nutrients, and deployment of autonomous Wirewalker drifting profilers near the eddy centers. This initial sampling was followed by Lagrangian, multi-day occupations of the eddy centers following Surface Velocity Program (SVP) drifters tracking near surface currents at 15 m depth, deployed near the centers of both eddies. Two Wirewalker drifting profilers were deployed near the SVP drifters to obtain vertically resolved observations of the upper 400 m at high temporal resolution. A more detailed description of sampling activities can be found in a companion manuscript (Barone et al., Under Revision). During the Lagrangian period, three sunrise to sunset (~14 hr) primary production experiments were conducted in each eddy using surface tethered arrays following established methods for the Hawaii Ocean Time-series (HOT). These were accompanied by longer term (89-hr) Fe amendment experiments on a separate array.

For all hydrographic parameters, sampling depths were converted to a mean isopycnal depth specific to each eddy center, which was calculated based on multi-day averages of potential density profiles determined from the

Wirewalkers. Daily integrals of downwelling photosynthetically active radiation (PAR) were calculated as the product of continuous measurements of surface PAR from a shipboard sensor (LI-COR LI-190), and the attenuation of PAR with depth, measured daily with a Hyperpro II optical profiler (Sea-Bird). Reported PAR values at the DCM are averaged from 5 m above and below the mean isopycnal depth of the DCM for each day, and then averaged across the 3-day Lagrangian sampling period.

2.2. Nutrient, Chlorophyll, and Flow Cytometry Analyses

Nutrient samples were collected using a rosette sampler and frozen immediately. Concentrations of nitrate + nitrite were analyzed by the high sensitivity chemiluminescent method described by Foreman et al. (2016), with a detection limit of 1 nM. Individual samples near the DCM of both eddies were also analyzed for nitrite using chemiluminescence (Foreman et al., 2016). Dissolved silicate was measured colometrically using a SEAL AA3 auto-analyzer (Strickland & Parsons, 1972; Wilson et al., 2019). Chlorophyll *a* was measured by the fluorometric method after acetone extraction (Lorenzen, 1967). Abundance of chlorophyll *a*, *b*, and *c* and divinyl chlorophyll *a* and *b* were measured by high performance liquid chromatography mass spectrometry (HPLC-MS) following procedures recently described by Becker et al. (2021). Abundance of picoeukaryotes, *Prochlorococcus*, *Synechococcus,* and heterotrophic bacterial cells were determined from samples preserved in 0.24% paraformaldehyde, flash frozen at $-80°C$ and analyzed by flow cytometry on an Influx flow cytometer (BD). Phytoplankton populations were identified by fluorescence and scattering properties. Heterotrophic (non-pigmented) populations were analyzed after staining with SYBR Green I, with phytoplankton contributions subtracted.

2.3. Dissolved Iron Sampling and Analysis

Trace metal sampling was conducted using a 12-position powder-coated "trace metal" rosette (SBE 32C with SBE 9plus CTD, Sea-Bird Electronics) mounted with 8 L externally sprung Niskin bottles (Ocean Test Equipment). The rosette was deployed on Spectra line using a metal-free block. All samples were processed in a HEPA-filtered, positive pressure trace metal clean "bubble" within a laboratory van. Bottles were filtered with an Acro-Pak 1500 cartridge filter (0.8 and 0.2 μm pore size) into 1 and 4 L LDPE bottles (Nalgene). All plasticware was rigorously cleaned by soaking in 2% Citranox overnight, followed by 1 week in a 10% hydrochloric acid (HCl) bath, and extensive rinsing with ultra-high purity water.

After returning to the laboratory, samples were acidified to pH 1.8 with 1 mL L^{-1} distilled HCl for several months. 15 mL aliquots were spiked with an isotope solution containing ^{57}Fe, ^{58}Fe, ^{62}Ni, ^{65}Cu, ^{110}Cd, and ^{111}Cd, extracted with Nobias PA-1 resin via a seaFAST preconcentration system (Elemental Scientific), and eluted in 3 M nitric acid with a 1 ppb Indium internal standard. Concentrations of Fe, Mn, Ni, Cu, and Cd were analyzed by Element 2 Inductively Coupled Plasma Mass Spectrometry (ICP-MS, Thermo Scientific) as previously described (Hawco et al., 2020). Preconcentration blanks (0.093 ± 0.015 nM Fe, $n = 29$) were subtracted from measured values. The accuracy of these measurements was confirmed by analysis of GEOTRACES community reference seawater samples GS (0.55 ± 0.01 nM Fe, $n = 3$) and GSP (0.19 ± 0.03 nM Fe, $n = 3$), which agree with current consensus values (GS: 0.546 ± 0.046 nM, GSP: 0.155 ± 0.045 nM, www.geotraces.org/standards-and-reference-materials).

2.4. Siderophore Analysis by HPLC-ICPMS and HPLC-MS/MS

Iron-binding ligands and siderophores were extracted from 4 L of 0.2 μm filtered seawater onto solid phase extraction columns at a flow rate of 20 mL min^{-1}. Prior to extraction, 6 mL Bond-Elut ENV columns (1 g, Agilent) were activated by passing 9 mL of high-purity methanol (Fisher Optima), 3 mL of 10 mM HCl, and 6 mL ultra-high purity water. Samples were then rinsed with 6 mL water, frozen at $-20°C$, and returned to the laboratory at Woods Hole Oceanographic Institution for processing. Immediately prior to analysis, columns were thawed and ligands were eluted with 12 mL methanol. Extracts were concentrated at 35°C to ~1.5 mL using a SpeedVac (Thermo Scientific). Aliquots were evaporated to dryness, and reconstituted in ultra-high purity water.

Iron ligands were analyzed using a Dionex Ultimate 3000 bioinert liquid chromatography system (Thermo Scientific) fitted with a C18 column (0.5 mm × 150 mm, 5 μm, Agilent). Compounds were eluted at a flow rate of 40 μL min^{-1} with a 20 min gradient from 5% to 90% solvent B, followed by a 10 min gradient from 90% to 95% solvent B, and a 5 min isocratic hold at 95% solvent B (solvent A: 5 mM aqueous ammonium formate, solvent B:

5 mM methanolic ammonium formate). Eluent was plumbed directly into a quadrupole ICP-MS (iCAP-Q, Thermo Scientific), using instrument settings described in Bundy et al. (2018). Instrument sensitivity was determined with a 4-point calibration curve of ferrichrome and ferrioxamine E standards. To identify siderophores, the liquid chromatography system was coupled to an Orbitrap Fusion mass spectrometer (Thermo Scientific) equipped with a heated electrospray ionization (H-ESI) source. Tentative identifications are made by comparison to known siderophore masses and retention times, as well as the presence of iron isotope pattern for siderophores bound to ^{54}Fe and ^{56}Fe. Ultra-high purity solvents and reagents were used throughout. Expanded details of this protocol are described in Boiteau and Repeta (2015).

2.5. Fe Amendment Incubations

Fe limitation of primary production was investigated with multi-day incubations conducted at *in situ* light and temperature conditions on a surface-tethered array. Seawater was collected from nighttime trace metal rosette casts and subsampled into cleaned 30 mL, 500 mL, and 2 L polycarbonate bottles (Nalgene) to determine bacterial production, primary production, and prokaryotic community structure (via 16S rRNA analyses), respectively. For Fe amended treatments (+Fe), 2 nM Fe was added directly to incubation bottles (as 5 μM FeCl$_3$ in a 10 mM HCl solution). At the DCM, additional treatments were also conducted using Fe bound to commercially available ferrioxamine B (Sigma) and amphibactin siderophores purified by HPLC from cultures of *Vibrio cyclitrophicus* 1F-53 following Boiteau et al. (2016). Siderophore-Fe complexes were added to final concentrations of 2 nM Fe with stock solutions stored at 4°C until use. The 500 mL and 2 L bottles were mounted on the array with custom-built acrylic frames and 30 mL bottles were placed in mesh bags and affixed to the array line. Dark incubations were conducted in vinyl dry-bags with pin-holes cut to allow exchange with surrounding waters with minimal light penetration. All processing was performed in the trace-metal-free bubble underneath HEPA-filtered workstations. Bottles were stored in coolers prior to deployment to minimize light and temperature perturbations during set up.

The arrays were deployed before sunrise and allowed to drift freely for 69 hr, when they were recovered (after sunset). At this point, 500 mL bottles were spiked with ^{14}C bicarbonate and 30 mL bottles were spiked with ^{3}H-leucine, prepared as described previously (Viviani & Church, 2017). Both radioisotope solutions were cleaned of metals using Chelex-100 resin (Bio-Rad; prepared according to Sunda et al., 2005) conditioned with unlabeled bicarbonate and leucine solutions at equal concentration. The 500 and 30 mL bottles were then re-affixed to the array, which was deployed prior to sunrise, ~73 hr after the start of the experiment. Incubations to measure primary and bacterial production continued until sunset (89 hr, an incubation time of 14 hr for the ^{3}H-leucine and ^{14}C uptake assays) when the arrays were recovered and measured according to established protocols (Viviani & Church, 2017). This duration is equivalent to the standard HOT program productivity measurements that also span dawn-to-dusk incubation periods. The 2 L bottles were harvested after initial recovery of the array (at 69 hr), filtered onto 25 mm 0.2 μm polyethersulfone filters, and preserved with RNA-later and frozen at −80°C. 16S rRNA genes were amplified from extracted genomic DNA with primers targeting the V4-V5 hypervariable regions and sequenced on an Illumina MiSeQ. Amplicon sequence variants were generated in DADA2 (Callahan et al., 2016). Full description is provided in Supporting Information S1.

Following the deployment of the *in situ* array, additional seawater from the DCM was collected in 2 L bottles and placed in incubators on deck (Caron Model# 7001-10) with light and temperature set to conditions matching the DCM in each eddy. Filtered control experiments were conducted in parallel and samples for HPLC-ICPMS analyses were collected after 5 days of incubation.

2.6. Transcriptome Searches

Metatranscriptome samples were collected at ~4 hr intervals for three days from isopycnal surfaces within the DCM during the Lagrangian sampling of the cyclonic (25.24 kg m^{-3}) and anticyclonic eddies (24.43 kg m^{-3}; $n = 18$ for each eddy). Procedures for filtration, preservation, addition of quantitative standards, sequencing and assembly followed published protocols (Gifford et al., 2016; Wilson et al., 2017) and are described fully in Supporting Information S1. *Prochlorococcus* iron responsive genes were identified from the culture experiments of Thompson et al. (2011). The abundance of gene transcripts (as copies mL^{-1}) were aggregated at the genus level

and then normalized to total *Prochlorococcus* transcripts. The statistical significance of the relative change in expression was tested using a Kruskal-Wallis test in the SciPy Python package (Virtanen et al., 2020).

2.7. Analysis of Hawaii Ocean Time-Series Datasets

HOT data from Station ALOHA were accessed using the Hawaii Ocean Time-series data organization and graphical system (HOT-DOGS: hahana.soest.hawaii.edu/hot/hot-dogs/), except for dFe data, which are replotted from Fitzsimmons et al. (2015). Direct comparisons to the MESO-SCOPE expedition are restricted to May – September months, while comparisons with PAR are conducted with monthly averages throughout the year (Karl et al., 2021). Monthly mean PAR values at specific depths are calculated as the product of the monthly averages of daily integrated irradiance at the ocean surface and the fraction of surface PAR at "standard" HOT depths.

3. Results and Discussion

3.1. Mesoscale Eddies as Natural Iron Fertilization Experiments to the Lower Euphotic Zone: Concepts and Predictions

Mesoscale eddies form from instabilities in large scale currents and can isolate waters for several months while transporting them hundreds of kilometers from their origin (Chelton et al., 2011; Zhang et al., 2014). The rotation of mesoscale eddies leaves a characteristic distortion in the corrected sea-level anomaly (SLA_{corr}; see Barone et al., Under Revision). Anticyclonic motions are associated with SLA maxima and accumulation of surface waters. Conversely, cyclonic eddies are associated with SLA minima and a depletion of surface water near the eddy center. Although there are myriad perturbations that can be encouraged by eddy activity (McGillicuddy, 2016), the most consistent feature of mesoscale eddies is the vertical displacement of density strata according to eddy polarity: cyclonic eddies lift denser waters upward, while anticyclonic eddies depress isopycnal surfaces downward (Barone et al., 2019; Siegel et al., 1999; Wunsch, 1997).

Mesoscale perturbation is of special relevance to the lower euphotic zone, where eddies alter the balance between light (largely a function of depth and light attenuation) and nutrient concentration (a function of density and vertical diffusivity) that influence phytoplankton growth in the DCM (Figure 1). Uplift of denser, nutrient-rich waters associated with cyclonic eddies can increase NO_3^- supply relative to a given light intensity (isolume),
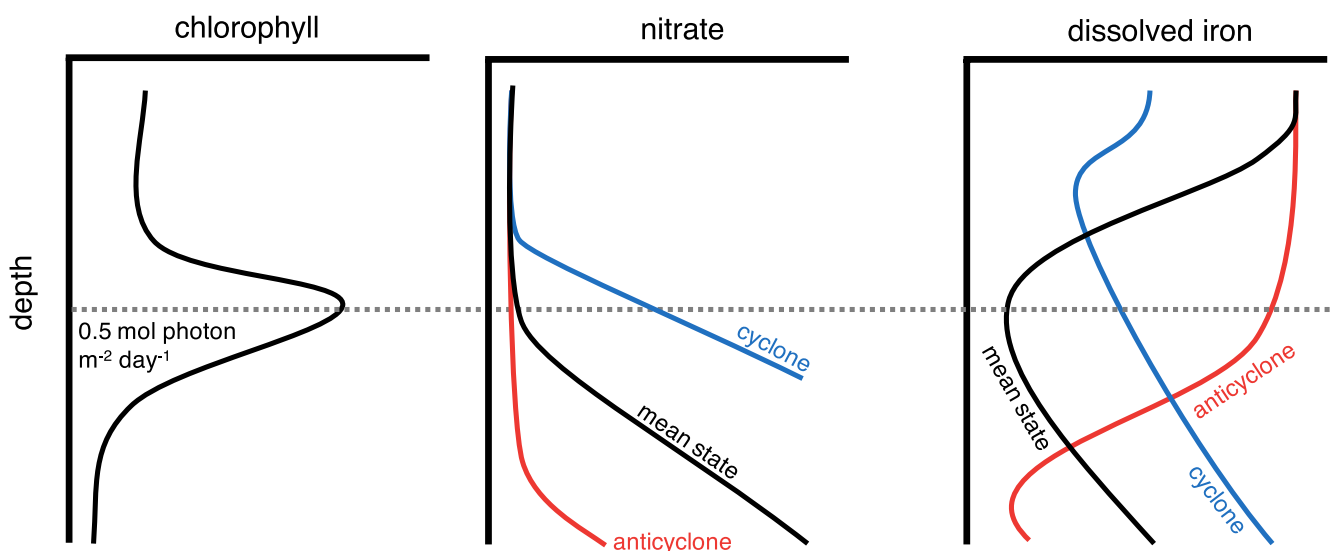
Figure 1. Idealized distributions of chlorophyll, nitrate, and dissolved iron in the North Pacific Subtropical Gyre (mean state, black lines). The deep chlorophyll maximum (DCM) is positioned close to the 0.5 mol photon m^{-2} day^{-1} isolume. Perturbations to the lower euphotic zone are induced by cyclonic (blue) and anticyclonic eddies (red). Downward motions in the anticyclone result in greater dFe concentrations at the DCM isolume while cyclonic eddies increase both dFe and nitrate. Note that surface dFe in the cyclone is predicted to be lower due to the uplift of low dFe waters at the initial DCM, but the changes in mixed layer dFe for both eddies depends on Fe sources from the atmosphere, as well as biological responses in the mixed layer affecting Fe uptake.

while anticyclones displace the nutricline downward, decoupling DCM isolumes from the diffusive supply of nitrate from below.

The effect of mesoscale perturbation can be separated into two conceptual stages: (a) the initial, physical perturbation and (b) the biological response to the physical perturbation. For the case of the cyclonic eddy, isopycnal uplift will shift the original DCM layer to shallower depths, where light absorption does not require the same degree of photoacclimation. Over time, the original DCM is expected to fade while a new DCM layer emerges underneath, near the 0.5 mol photon m^{-2} day^{-1} optimum that supported the DCM prior to perturbation (Letelier et al., 2004). For the anticyclone, the original DCM will be positioned too deeply for photosynthesis to remain viable, leading to the development of a new DCM in shallower waters that approach the 0.5 mol photon m^{-2} day^{-1} isolume. For either eddy type, biological responses in the mixed layer may further modulate the positioning of the DCM by increasing light attenuation in the overlying water column.

Because the original DCM overlaps with a minimum in dFe, with concentrations increasing both above and below, regrowth of the DCM within a mesoscale eddy will occur in waters with higher dFe (Figure 1). The cyclonic eddy DCM will regrow in an environment that now hosts higher dFe from the nutricline, in addition to higher NO_3^-. In contrast, an anticyclone DCM will regrow within lower density waters, containing elevated dFe originating from the surface but with potentially lower NO_3^-. Thus, for eddies that are sufficiently long-lived, re-equilibration of the lower euphotic zone ecosystem will occur in distinct nutrient regimes: the centers of anticyclones resemble an Fe addition without NO_3^-, while cyclones represent a simultaneous addition of Fe and NO_3^- (Figure 1). From this, we hypothesize that both eddy types would relieve iron limitation at the DCM, if it occurred, and would increase primary production and carbon export relative to baseline values at similar isolumes. In contrast, prevalence of nitrogen limitation would favor a productivity increase within cyclonic eddies only. The ecosystem response to mesoscale forcing may therefore reveal the extent of iron limitation at the DCM in the mean state.

3.2. Iron, Nutrient, and Phytoplankton Perturbations Along an Eddy Dipole

During July 2017, we examined the biogeochemistry of a cyclonic-anticyclonic eddy pair in the central North Pacific Subtropical Gyre (Figure 2). A more detailed description of the 2017 MESO-SCOPE expedition is presented by Barone et al. (Under Revision). Satellite tracking of both eddies suggested a similar point of origin northeast of Hawai'i, with estimated ages of 100 days for the cyclonic eddy and 140 days for the anticyclone. At the time of their sampling, these eddies were near their peak SLA: +24 and −15 cm for the anticyclone and cyclone, respectively (Figure 2a). Eddy centers were associated with large perturbations to the density structure of the upper ocean, with an eddy-to-eddy difference of ~120 m for the depth of the 25.0 kg m^{-3} isopycnal anomaly (σ_θ), which falls within the nitracline at Station ALOHA (1.9 ± 0.9 μM NO_3^-, 190 m mean depth; Figure 2b). In contrast, the position of the DCM between eddy centers varied by less than 20 m, corresponding to 25.2 kg m^{-3} in the cyclonic eddy (104 m depth) and 24.4 kg m^{-3} in the anticyclone (118 m). Multi-day integrals of PAR indicated that the DCM of both eddies occurred at a similar light flux: 0.46 ± 0.18 and 0.29 ± 0.02 mol photon m^{-2} day^{-1} for the cyclonic and anticyclonic eddies, respectively (Table 1). While these irradiance estimates fall slightly below the canonical value of 0.5 mol photon m^{-2} day^{-1} (Letelier et al., 2004), they suggest that the eddies sampled in 2017 were sufficiently mature and stable to allow for biological re-equilibration of the lower euphotic zone to an optimal irradiance.

The ecosystem response to eddy-driven perturbations left clear signatures in nutrient inventories. At 200 m depth (below the photosynthetic compensation irradiance), isopycnal uplift in the cyclonic eddy led to NO_3^- concentrations of 7.65 μM, an order of magnitude greater than observed in the anticyclonic eddy at the same depth (0.69 μM; Figure 3). Most of this difference in NO_3^- could be accounted for solely by the vertical displacement of water masses. As a result, variability decreased substantially when eddy center profiles were compared against density (Figure 3). Similar depth offsets were observed for profiles of dissolved Ni, Cu, and Cd, and Mn, which also realigned when plotted against density (Figure S1 in Supporting Information S1). However, between 25.0 and 25.3 kg m^{-3}, the cyclonic eddy contained 1–3 μM less NO_3^- than the anticyclonic eddy. This density range overlapped with a large population of small eukaryotic phytoplankton (picoeukaryotes; up to 5×10^3 cells ml^{-1}) in the cyclonic eddy DCM and a decrease in *Prochlorococcus* abundance (Figure 4). Although *Prochlorococcus* is typically responsible for most of the productivity, biomass, and chlorophyll near the DCM in this region (e.g., at Station ALOHA; Rii et al., 2016), the *Prochlorococcus*-specific pigments divinyl chlorophyll *a* and *b* were
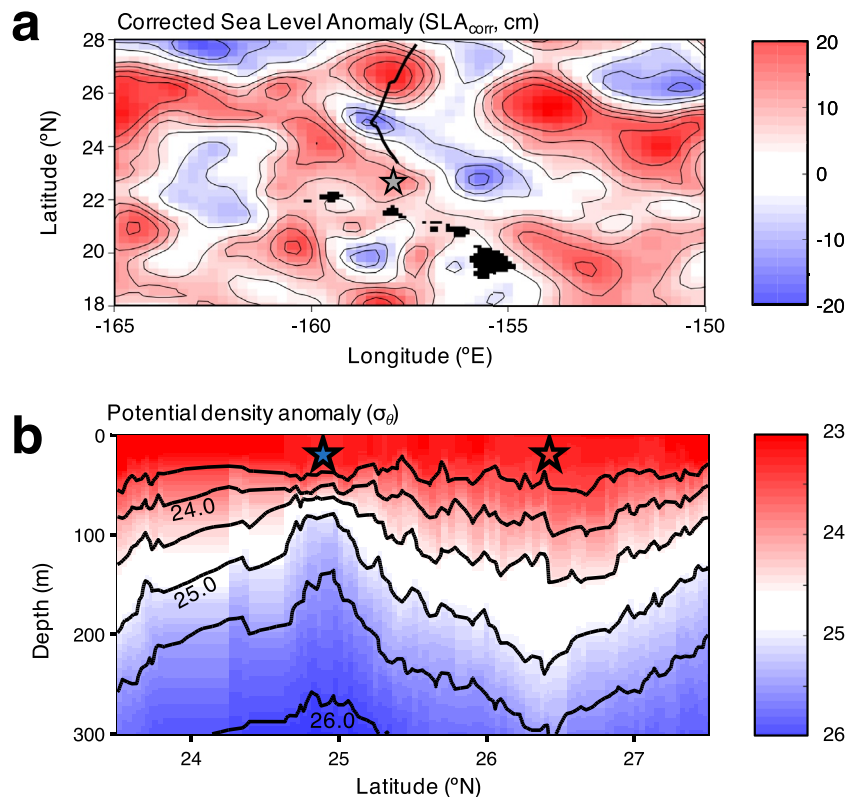
Figure 2. Characterization of an eddy dipole in the North Pacific Subtropical Gyre during July 2017. (a) Corrected sea-level anomalies (SLA$_{corr}$) across the region. Blue shading highlights minima in SLA$_{corr}$, marking cyclonic eddies, while SLA$_{corr}$ maxima (red) coincide with anticyclones. Contours mark 5 cm intervals, excluding 0 cm (white shading). (b) A section of potential density anomaly (σ_θ) following the bold line of the cruise track in Figure 2a. Uplift of dense isopycnal surfaces (blue shading) peaks at 24.9°N and depression of surface water masses (red shading) is greatest at 26.4°N. Blue and red stars indicate stations occupied for hydrographic sampling in the cyclonic and anticyclonic eddy centers, respectively. The gray star in Figure 2a indicates the location of Station ALOHA.

exceeded by chlorophylls *a*, *b* and *c* in the cyclonic eddy DCM, the latter three representing ~60% of total chlorophyll and primarily reflecting eukaryotic phytoplankton (*Synechococcus* and other cyanobacteria were much less abundant; Table 1). Among larger cells (>4 μm), haptophytes were the strongest contributors to the increase in eukaryotic biomass in the cyclonic eddy DCM, with smaller contributions from diatoms, dinoflagellates and chlorophytes (Barone et al., Under Revision). We note that isopycnal comparisons indicate little Si drawdown in the cyclonic eddy center (Figure S2 in Supporting Information S1). In the anticyclone, *Prochlorococcus* accounted for 58% of total chlorophyll at the DCM. Together, these observations suggest that uplift of nutrient-rich waters into the lower euphotic zone enabled significant biological uptake of NO$_3^-$ in the cyclonic eddy, primarily by eukaryotic phytoplankton, consistent with the predictions of the conceptual model.

In contrast, the depth profile of dFe in the cyclonic eddy resembled profiles in the anticyclonic eddy and under non-eddy conditions at Station ALOHA. Each of these profiles contained a minimum at the DCM (Figure 3d), despite the fact that the DCM of the cyclonic eddy occurred on a distinct isopycnal surface that is usually associated with elevated Fe from remineralization (Figure 3h). Indeed, dFe at 25.25 kg m^{-3}—within the DCM of the cyclonic eddy—was 63 pM, compared to 170 pM in the anticyclone at a similar density (25.15 kg m^{-3}, 250 m depth). The latter value is similar to an average dFe of 152 ± 46 pM between 175-250 m depth at Station ALOHA (Fitzsimmons et al., 2015), corresponding to a range of σ_θ between 24.9 and 25.5 kg m^{-3}. Thus, NO$_3^-$ uptake in the cyclonic eddy coincided with dFe uptake on the order of 100 pM. While the anticyclone also had a minimum in dFe at the DCM, this concentration (~136 pM) was roughly double the dFe measured in the cyclone and at Station ALOHA (Table 1), likely reflecting downwelling of dFe from surface waters.

Table 1

Attributes of the Deep Chlorophyll Maximum (DCM) in the Cyclonic and Anticyclonic Eddies Observed During the 2017 MESO-SCOPE Expedition

Parameter	MESO-SCOPE, June – July 2017		HOT, May – September Station ALOHA[a]
	Cyclone	Anticyclone	
Latitude, longitude (°N, °W)	24.86, 158.57	26.37, 158.01	22.75, 158.0
Sea level anomaly (SLA_{corr}, cm)	−18	+25	+0.9
Density anomaly (σ_θ, kg m^{-3})	*25.22*	*24.37*	24.23/24.67
Mean isopycnal depth (m)	*104*	*118*	100/125
Chlorophyll *a* (µg L^{-1})	0.32 (*0.26*)	0.19 (*0.22*)	0.21/0.19
Light (PAR, mol photon m^{-2} day^{-1})	*0.46 ± 0.18*	*0.29 ± 0.02*	0.5[b] (0.74/0.23 [a])
Primary production (µM C day^{-1})	*0.21 ± 0.03*	*0.10 ± 0.01*	0.12 ± 0.04[c] (0.21/0.07 [a])
Nitrate + Nitrite (nM)	820	3	25/230
Nitrite (nM)	79	<3	2/45
Phosphate (nM)	168 (*145*)	85 (*77*)	62/95
Silicate (nM)	3,300	1,900	1,380/1,580
Dissolved Iron (dFe, pM)	63	136	66 ± 21[d]
Dissolved Mn (pM)	620	1,390	1,250[e]
dFe:NO$_3$ supply ratio (µmol:mol)[f]	50.4	215	87–100
Picoeukaryotes (cells ml^{-1})	*4,080*	*2,700*	1,200/1,200
Prochlorococcus (cells ml^{-1})	*69,700*	*97,000*	158,000/68,000
Synechococcus (cells ml^{-1})	*530*	*<100*	1,000/300
Heterotrophic bacteria (cells ml^{-1})	*496,000*	*423,000*	389,000/316,000

Note. Values in italics derive from the Lagrangian observation period at the eddy centers. May – September average values from Station ALOHA at 100 m and 125 m are shown for comparison, separated by a slash.

[a]Average values at 100 and 125 m obtained from the HOT-DOGS online database. [b]Letelier et al. (2004). [c]Average for all month/depth combinations with an irradiance between 0.2 and 0.6 mol photon m^{-2} day^{-1}. [d]Obtained from Fitzsimmons et al. (2015), averaged over 90–130 m depth range. [e]Boyle et al. (2005) from MP5 cruise (1 July 2002). [f]Calculated as the sum of upward (DCM to 250 m) and downward (surface to DCM) dFe/dz relative to upward (DCM to 250 m) dNO$_3$/dz, assuming similar diffusive mixing above and below the DCM.

3.3. Direct Tests of Fe Limitation in the Lower Euphotic Zone

To determine the influence of the eddy perturbation on ecosystem productivity, primary production was measured during a period of Lagrangian sampling in the centers of both eddies (Figure 5). Consistent with isopycnal evidence for uptake of NO$_3^-$ and dFe, rates of primary production in the DCM (by the ^{14}C method) were moderately higher (0.21 ± 0.03 µM C day^{-1} between an irradiance of 0.2–0.6 mol photon m^{-2} day^{-1}, $n = 4$) compared to rates at equivalent PAR in the anticyclonic eddy (0.10 ± 0.01, $n = 2$) or average values from Station ALOHA (0.12 ± 0.04 µM C day^{-1}, Table 1). This amounts to a doubling of productivity within the DCM, but the effect is small compared to the large increase in ^{14}C uptake at all sites with increasing light (Figure 5). Similar relationships between irradiance and primary production in the anticyclone and at Station ALOHA suggest that the two-fold increase in dFe at the anticyclonic eddy DCM did not stimulate primary production.

Longer term incubations were conducted to evaluate the sensitivity of primary production to dFe. After 3 days of incubation *in situ*, unamended control incubations in the cyclonic eddy harbored an unusual maximum in ^{14}C uptake at 100 m depth, just above the DCM, equal to 0.43 ± 0.04 µM C day^{-1} (mean ± 1 standard deviation of 3 bottle replicates; Figure 6). This rate is more than double the productivity observed in shorter term experiments at 100 m (0.21 µM C day^{-1}) and 3 standard deviations above mean May–September primary production at 100 m for Station ALOHA (0.21 ± 0.07 µM C day^{-1}; nearly equal to the maximum rate of 0.55 µM C day^{-1} over the entire record at 100 m). The higher productivity in the longer term experiments could be evidence of reduced grazing pressure within the incubated bottles, allowing biomass to increase. Iron addition to bottles incubated at this
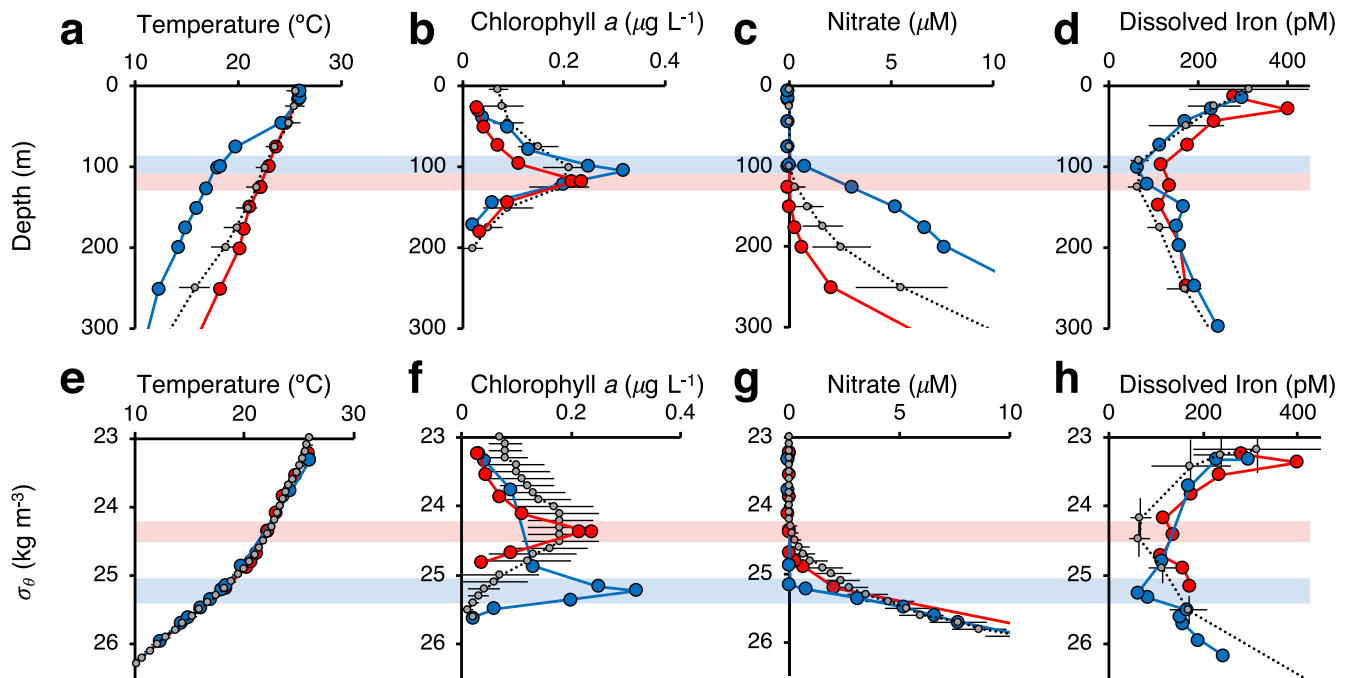
Figure 3. Perturbation of water column properties in cyclonic (blue lines) and anticyclonic (red lines) eddy centers as a function of (a–d) depth and (e–h) potential density anomaly (σ_θ). Long term averages for May–September observations from Station ALOHA, located nearby, are plotted in gray. Decoupled depth profiles of temperature (a) collapse when plotted against density (e). The deep chlorophyll maximum (DCM) occurs at a similar depth (b) in both eddies but on distinct density surfaces (f) and coincides with removal of nitrate (c and g) and dissolved Fe (d and h) at the cyclonic eddy DCM. The DCM of each eddy is marked in all panels by red and blue shading.

depth increased primary production slightly to 0.54 ± 0.08 µM C day^{-1}, but not significantly ($p > 0.05$, Student's t-test). At the DCM of the cyclonic eddy (incubated at 110 m), primary production was lower: 0.25 ± 0.05 µM C day^{-1} in the control and 0.27 ± 0.07 µM C day^{-1} in the 2 nM Fe treatment, similar to the short term productivity measurements from the DCM (0.22 ± 0.04 µM C day^{-1}). Equivalent primary production was also observed in control and +Fe treatments throughout the lower euphotic zone of the anticyclone (Figure 6). Additions of Fe as Fe-amphibactin D or ferrioxamine B siderophores also did not increase DCM primary production relative to the unamended control in either eddy center (Figure S3 in Supporting Information S1).

Although primary production did not change significantly following Fe addition, Fe did increase rates of ^{3}H-leucine incorporation at both 100 and 110 m in the cyclonic eddy. At 100 m, leucine incorporation under ambient

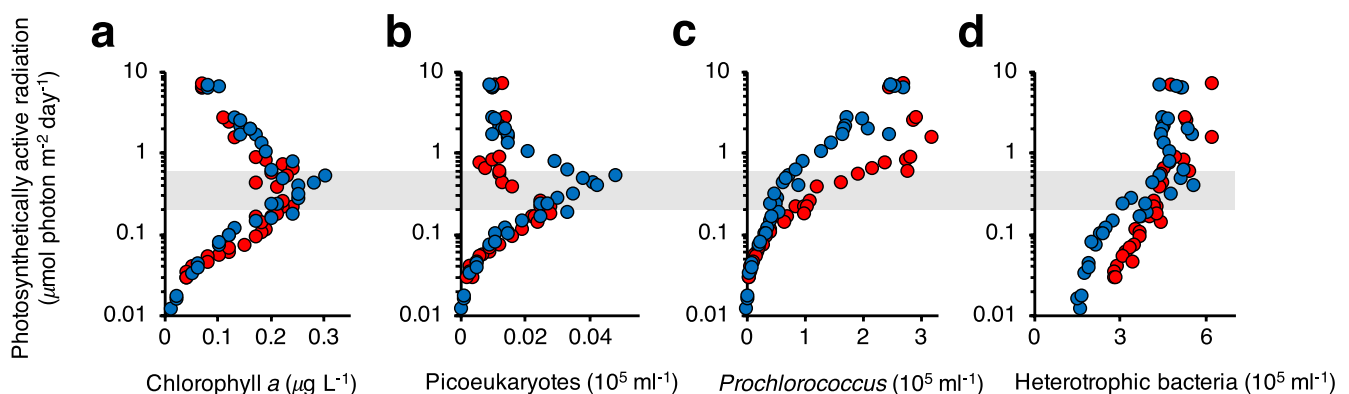**Figure 4.** Alignment of (a) chlorophyll *a*, (b) picoeukaryotes, (c) *Prochlorococcus*, and (d) heterotrophic bacteria by ambient light (as photosynthetically active radiation, PAR) in the cyclonic (blue) and anticyclonic (red) eddies. The gray shading highlights the range in PAR associated with the DCM in both eddies (0.2–0.6 µmol photon m^{-2} d^{-1}), which also encompasses the DCM at Station ALOHA.
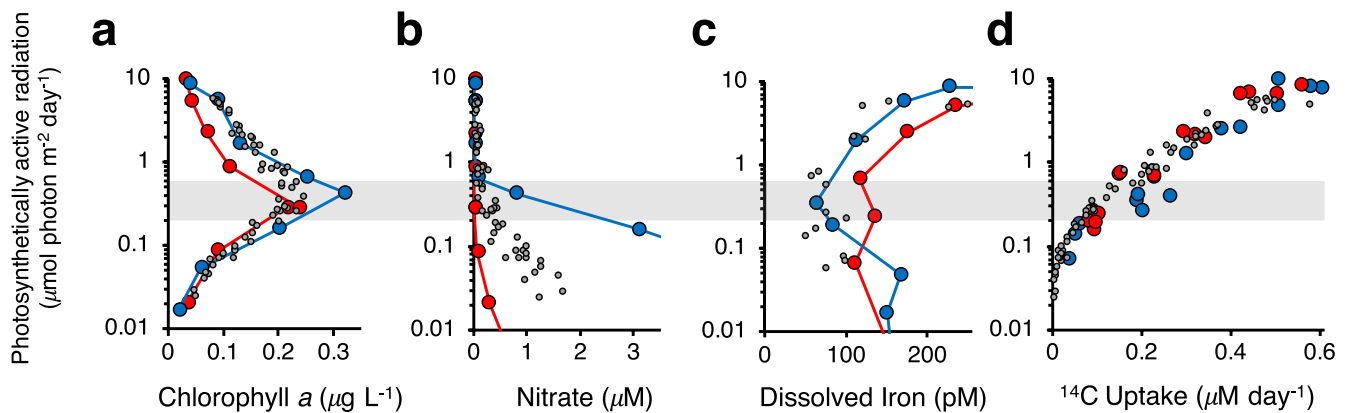
Figure 5. Intercomparison of nutrients, iron, productivity, and light. Cyclonic (blue) and anticyclonic (red) eddy center profiles of (a) chlorophyll *a*, (b) nitrate, (c) dissolved iron from Figure 3, and (d) rates of ^{14}C uptake from three separate 14-hr (sunrise to sunset) incubations at *in situ* temperature and light during the Lagrangian period. Each circle for ^{14}C uptake represents the mean of triplicate incubations. Monthly averaged data from Station ALOHA are plotted as gray circles. Note that these 14-hr primary production measurements are distinct from the multi-day experiments in Figure 6.

light increased from 15.7 ± 1.8 pM hr^{-1} (control) to 23.5 ± 2.2 pM hr^{-1} (+Fe; $p < 0.05$, Student's t-test; Figure 6b). A considerably smaller increase was observed in dark incubations at this depth (13.3 ± 1.2 vs. 15.4 ± 0.08, Figure S3 in Supporting Information S1). At the DCM (110 m), Fe also increased rates of ^3H-leucine incorporation ~30% above unamended controls under ambient light. Analysis of the bacterial community at 100 and 110 m by amplification and sequencing of 16S rRNA genes indicated dominance of *Prochlorococcus* and *Pelagibacter*, but community composition in ambient light incubations did not differ significantly between controls and +Fe treatments (Figure 6c). Compared to observations at Station ALOHA (Viviani & Church, 2017), rates of ^3H-leucine incorporation were high throughout the euphotic zone of the cyclonic eddy, possibly reflecting the same relief of grazing pressure that led to higher ^{14}C uptake in long term incubations. Alternatively, elevated rates could be explained by microbial succession following high initial productivity and export during the intensification phase of this eddy (Barone et al., Under Revision).

In the anticyclone, rates of ^3H-leucine incorporation were similar to observations at Station ALOHA, and lower throughout the water column compared to the cyclonic eddy. Leucine incorporation was not stimulated with Fe
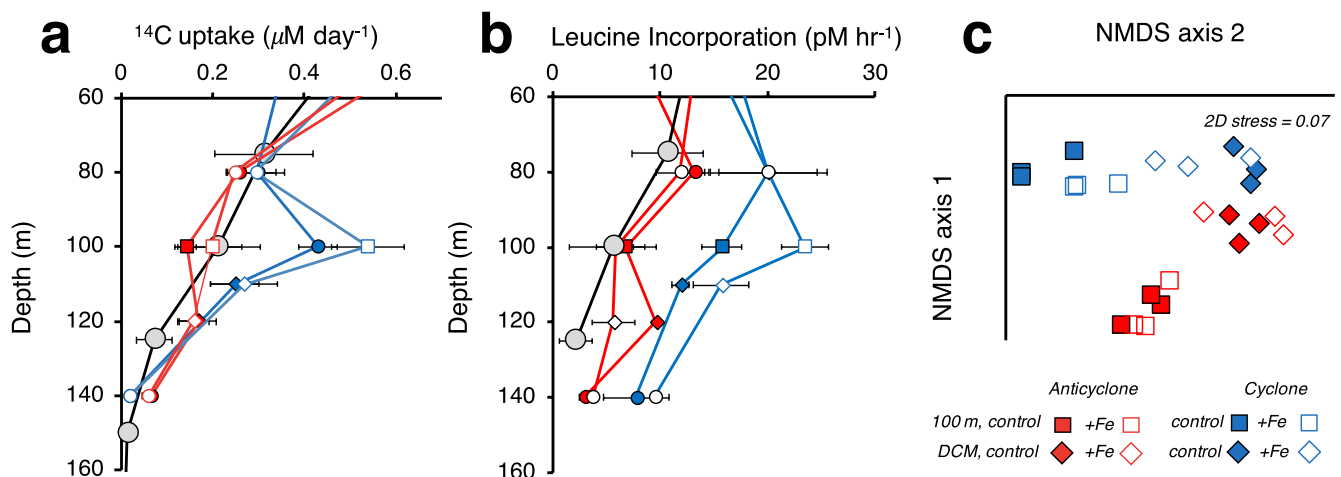
Figure 6. Tests of iron limitation in the cyclone (blue) and anticyclone (red) centers. Following 3 days of incubation at *in situ* light and temperature, (a) ^{14}C uptake and (b) leucine incorporation assays were conducted for unamended seawater (filled symbols) and 2 nM Fe additions (open symbols) from sunrise to sunset. Experiments at 100 m (squares) and the DCM (diamonds) of the cyclonic eddy show a significant response for leucine incorporation in +Fe experiments relative to controls. Gray circles show May – September values from Station ALOHA. (c) Non-metric multi-dimensional scaling (NMDS) ordination of 16S rRNA gene amplicon sequences from *in situ* incubations indicate distinct communities in each eddy and at each depth, but limited change due to Fe addition. NMDS based on weighted UniFrac distance matrix of amplicon sequence variants.

Figure 7. (a) HPLC-ICPMS chromatograms of Fe-binding ligands in the deep chlorophyll maximum (DCM) of the cyclonic and anticyclonic eddies (blue and red lines, respectively), and from 250 m in the anticyclonic eddy (pink line). The 250 m anticyclone sample corresponds to a similar density as the cyclonic eddy DCM. Early elution of ferrioxamines (ca. 15 min) is highlighted in comparison to later elution (25–30 min) of amphibactins and other non-polar siderophores. (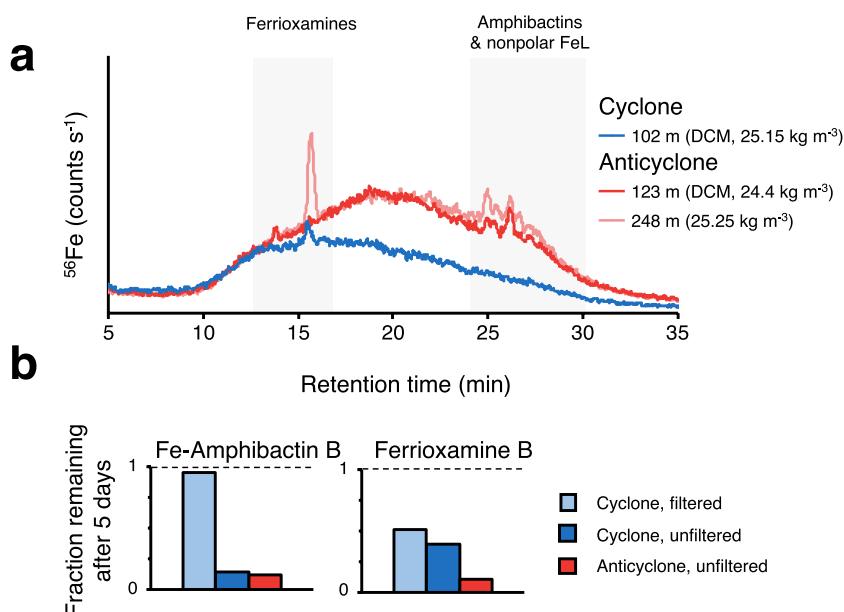b) On-deck incubation experiments showing loss of Fe-amphibactin D or Ferrioxamine B added to DCM waters from the cyclonic eddy (blue bars) and anticyclonic eddy (red bars) after 5 days of incubation. Filtered control experiments (light blue bars) were only conducted in the cyclonic eddy, and suggest significant abiotic loss of ferrioxamine B but not Fe-amphibactin D.

addition at 100 m, nor at the DCM (120 m), consistent with greater dFe in the anticyclonic eddy ($p > 0.05$, one-way ANOVA). Despite distinct prokaryotic communities between eddies and between 100 m and the DCM (Figure 6c), no significant changes in community structure (based on rRNA gene analysis) were observed following Fe addition in the anticyclone.

3.4. Mesoscale Perturbation of Siderophore Distributions and Cycling

Most dFe in the upper ocean is strongly bound to organic ligands, including siderophores, which cycle at an unknown rate. Prior measurements of excess Fe ligand concentrations in the North Pacific Subtropical Gyre appear invariant over the upper 300 m (Fitzsimmons et al., 2015), but siderophores with unique depth distributions have been identified throughout the water column at Station ALOHA (Bundy et al., 2018). In the eddy dipole, HPLC-ICPMS analyses highlighted significant shifts in Fe speciation between eddies. Both eddies displayed an unresolved complex mixture of Fe ligands that appear as a hump in the chromatogram baseline (Figure 7a). Within each eddy, these unresolved ligands were roughly constant with depth, but were greater in the anticyclone (44 ± 5 pM) compared to the cyclone (17 ± 2 pM). Identified ligands in the anticyclone included the high-affinity and polar siderophore ferrioxamine-E and a suite of amphibactins, which are non-polar and have weaker binding affinity for Fe (Bundy et al., 2018). In the cyclonic eddy, ferrioxamine-E was the most abundant siderophore, but total siderophores averaged over 0–150 m were much lower (0.3 pM) compared to the anticyclonic eddy (2.6 pM). Indeed, siderophore concentrations in the cyclonic eddy DCM (0.13 pM) were 15-fold lower than at a corresponding density in the anticyclone (2.0 pM at 250 m), perhaps reflecting uptake of these compounds following uplift into the euphotic zone (Figure 7a). The differences in dFe and siderophore abundances in the cyclonic and anticyclonic eddies suggest that their turnover times in the upper ocean are fast relative to the lifetimes of these eddies (estimated to be 100 days or more).

To estimate the rate of siderophore cycling, parallel incubations were also performed on deck with 2 nM ferrioxamine B and Fe-amphibactin D added to DCM waters from both eddies. After 5 days of incubation at similar light and temperature, concentrations of ferrioxamine B and Fe-amphibactin D in waters from the cyclone DCM

decreased by 61% and 86%, respectively (Figure 7b). However, ferrioxamine B added to a 0.2 μm filtered control experiment also decreased by 49%, indicating that part of the loss in the unfiltered experiments was due to abiotic factors (e.g., hydrolysis, chelate dissociation, or adsorption to bottle walls). In contrast, 95% of added Fe-amphibactin D was recovered in the filtered controls, indicating that its removal from unfiltered incubations was primarily due to biological activity. Similar levels of amphibactin D removal (88%) were also found in the anticyclonic eddy, where greater ferrioxamine B removal was observed (90%). These experiments provide evidence that amphibactins represent a readily bioavailable Fe source to the microbial community, which is consistent with the uptake inferred in the cyclonic eddy DCM based on isopycnal comparisons (Figure 7a). Yet, amphibactins may not be bioavailable to the entire microbial community: addition of 2 nM Fe-amphibactin D did not increase ^{3}H-leucine incorporation in the cyclonic eddy DCM, despite the increase observed with addition of unchelated Fe (Figure S3 in Supporting Information S1). Overall, there is a need to constrain the bioavailability and turnover times of these siderophores, especially the roles of heterotrophic uptake and abiotic degradation that could limit their longevity below the euphotic zone.

3.5. *Prochlorococcus* Fe Limitation in the Cyclonic Eddy?

The physical perturbation of the anticyclonic eddy can be conceptualized as an Fe fertilization to the DCM (Figure 1). By the time this eddy was sampled, the DCM had repositioned near the 0.5 mol photon m^{-2} day^{-1} isolume, with residual dFe concentrations that were significantly greater than observed at Station ALOHA (Figures 3 and 5). Yet, this apparent increase in dFe was not matched by increased primary productivity (by ^{14}C uptake) or ^{3}H-leucine incorporation relative to measurements at Station ALOHA (Figures 5 and 6). Additional evidence for a significant biological response in the lower euphotic zone (e.g., O_2 accumulation or increases in sinking organic matter flux) is also lacking in this eddy (Barone et al., Under Revision). The simplest explanation for these observations is the absence of a bioavailable nitrogen source that would allow biomass and/or productivity to increase beyond typical values, but this implies that any effect of iron on DCM productivity first requires an adequate N supply, likely ruling out proximal Fe-limitation under non-eddy conditions.

Simultaneous N and Fe inputs did occur in the center of the cyclonic eddy, which hosted increased primary production near the DCM. Increased nutrient delivery to DCM isolumes is consistent with the emergence of picoeukaryotes, which can grow rapidly with a NO_3^- source, and the decline of *Prochlorococcus* (Figure 4), often considered to grow solely on reduced N sources (e.g., ammonia, urea, and amino acids; Moore et al., 2002). Despite this conception, genomic analyses have found that genes for nitrate reductase are widespread in LL1 *Prochlorococcus* ecotypes, whose abundance peaks near the DCM at Station ALOHA (Berube et al., 2016, 2019; Casey et al., 2007; Malmstrom et al., 2010). Thus, increased NO_3^- supply may still allow an increase in *Prochlorococcus* biomass.

Relatively high iron requirements for *Prochlorococcus* photosynthesis may make them less competitive when NO_3^- supply increases. Experiments under DCM conditions with a low-light adapted *Prochlorococcus* (MIT1214 strain, LL1 ecotype) have indicated that the onset of Fe limitation is associated with an Fe:C ratio of 30–40 μmol:mol (Hawco et al., 2021), which is similar to the HLI *Prochlorococcus* strain MED4 when grown under low light (~45 μmol:mol; Cunningham & John, 2017; Shire & Kustka, 2015). In the center of the cyclonic eddy, removal of 100 pM dFe was associated with the uptake of 2 μM NO_3^-. Assuming a C:N ratio of 6.6, the corresponding Fe:C ratio, 8 μmol:mol, is below these *Prochlorococcus* Fe:C thresholds, suggesting that NO_3-dependent growth in the cyclonic eddy would lead to Fe limitation. In contrast, some eukaryotic phytoplankton can grow at low irradiance with an Fe:C ratio below 5 μmol:mol (Maldonado & Price, 1996; Marchetti et al., 2006; Strzepek et al., 2012), likely because eukaryotic cells are able to support larger chlorophyll antennae than *Prochlorococcus*, decreasing the required number of photosynthetic reaction centers at low light (Bibby et al., 2003; Hawco et al., 2021; Strzepek et al., 2019). Lower photosynthetic Fe requirements among eukaryote phytoplankton could therefore allow NO_3^- drawdown without Fe limitation. While this reasoning applies mostly to the intensification stage of the cyclonic eddy where heightened export occurred (taking place prior to our observations; Barone et al., Under Revision), persistent and steep NO_3^- gradients imply that diffusive mixing maintained a similar Fe:NO_3 supply ratio during the mature phase of this eddy (~7.6 μmol Fe: mol C when converted with a 6.6 C:N ratio; see Table 1), which would support the continued growth of well-adapted picoeukaryotes without forcing Fe limitation.
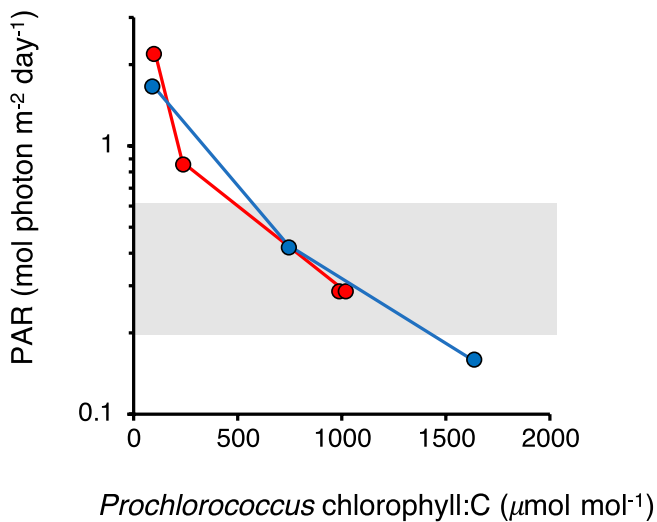
Figure 8. Estimated chlorophyll:C ratios of *Prochlorococcus* cells in the lower euphotic zone in the cyclone (blue) and anticyclone (red). Circles represent measurements conducted during the hydrographic survey, matching Figures 3 and 5. Chlorophyll:C ratios are calculated as the sum of divinyl chlorophyll *a* and *b*, which are diagnostic of *Prochlorococcus,* with cell number converted to cell C assuming 4 fmol C per *Prochlorococcus* cell. Gray shading highlights the DCM region in both eddies as per Figures 4 and 5.

The primary evidence for Fe stress within the cyclonic eddy comes from greater leucine incorporation when iron was added to multi-day incubations, especially in bottles receiving ambient light. ^{3}H-Leucine incorporation assays have a long history of tracing heterotrophic production, but rates in the lower euphotic zone can increase significantly when exposed to ambient light due to increased uptake and incorporation by phototrophs (Church et al., 2006). At Station ALOHA, *Prochlorococcus* can account for 60% of leucine incorporation under ambient light despite being outnumbered by heterotrophic bacteria. In dark incubations, the *Prochlorococcus* contribution decreases to ~20% (Björkman et al., 2015). Therefore, the Fe stimulation of leucine incorporation in the cyclonic eddy could reflect enhancement of *Prochlorococcus* activity that was not apparent (or statistically resolvable) in bulk ^{14}C uptake. At 100 m, the relative Fe stimulation effect was much greater in the light (~50%) than the dark (16%), consistent with the magnitude of *Prochlorococcus*-driven incorporation at Station ALOHA (Björkman et al., 2015). Because NO_3^- uptake and reduction via the nitrate reductase enzyme is expected to increase Fe requirements (Raven, 1988), *Prochlorococcus* leucine incorporation may be motivated by acquisition of reduced nitrogen rather than organic carbon (Björkman et al., 2015; Duhamel et al., 2018). Stimulation of *Prochlorococcus* metabolism is also consistent with their abundance in these incubations: 16S rRNA gene amplicon sequencing of +Fe and control treatments did not provide evidence for emergence of a new population of possibly Fe-limited heterotrophic bacteria (Figure 6c), suggesting that the leucine incorporation signal is driven by a population that was already dominant (e.g., *Pelagibacter*, *Prochlorococcus*).

However, there are also potential experimental artifacts for the multi-day incubations that can complicate comparisons to the surrounding seawater. At a fixed depth, these incubations provide an incomplete representation of the dynamic light fields caused by inertial waves and other physical processes, which result in vertical oscillations with periods of hours to days (Letelier et al., 1993). Bottled phytoplankton are also isolated from numerically rare and vertically migrating grazers. Relief from grazing pressure over several days could support increases in autotrophic biomass and explain why the large productivity maximum at 100 m in the multi-day incubations was not found in multiple 12-hr ^{14}C productivity measurements in the same eddy. We speculate that if isolation from protistan grazers and zooplankton allowed the biomass of some phytoplankton to increase, it would also have reduced the recycling of biomass Fe needed to sustain the growth of *Prochlorococcus*, enabling the observed Fe stimulation of leucine incorporation.

Indeed, we were unable to find strong evidence for *Prochlorococcus* Fe stress under background conditions. Like other phytoplankton, the onset of Fe limitation in *Prochlorococcus* in culture is associated with a decrease in the Chl:C ratio (Hawco et al., 2021; Sunda & Huntsman, 1997). In both eddies, there is a similar relationship between PAR and derived *Prochlorococcus* Chl:C, calculated as the sum of divinyl chlorophyll *a* and *b*, which are both specific to *Prochlorococcus*, using a uniform mol C cell^{-1} conversion (Figure 8). This comparison indicates that *Prochlorococcus* photoacclimation is not strongly impacted by the low dFe in the cyclonic eddy. We also searched for known Fe stress markers from transcriptomes sampled in the DCM throughout the Lagrangian observation period. Iron limitation is expected to up-regulate expression of *isiB*, which encodes the electron carrier flavodoxin that substitutes for Fe-containing ferredoxin in photosynthetic electron transport, the latter encoded by the *petF* gene (Bibby et al., 2003; Thompson et al., 2011). Expression of *isiB* was slightly increased in the cyclonic eddy compared to the anticyclonic eddy, while *petF* was slightly decreased (Table 2). The resulting ~2-fold increase in the *isiB*:*petF* ratio in the cyclonic eddy follows the direction anticipated by Fe stress, but falls short of the >10-fold change expected from culture studies of both high- and low-light adapted *Prochlorococcus* strains (Thompson et al., 2011). Similarly, the small (17%) increase in expression of the *idiA* gene, encoding the periplasmic Fe binding component of the iron ABC transporter, in the cyclonic eddy matches the direction but not the magnitude identified in culture (>500%). Of these genes, only *petF* (ferredoxin) met significance criteria used to identify differential expression between the two eddies ($p = 0.046$, Table 2). Given the muted response of

Table 2
Abundance of Prochlorococcus Nutrient Stress Gene Markers Based on Transcriptomes From the Deep Chlorophyll Maximum (DCM) of Both Eddies

Gene product	Expected iron stress response?	Mean DCM expression (copies ml^{-1})		Normalized C:A ratio
		Cyclone	Anticyclone	
Fe binding protein (*idiA*, COG1840)	Upregulation[a]	14,000	9,900	1.17
Flavodoxin (*isiB*, COG0716)	Upregulation[a]	77,000	60,000	1.08
Ferredoxin (*petF*, COG0633)	Downregulation[a]	6,800	10,400	0.54*
Ferritin (COG1528)	Downregulation[b]	15,000	14,000	0.89
Photosystem II D1 (*psbA*, ENOG502Z87P)		520,000	510,000	0.86

Note. The ratio of transcripts in the cyclonic versus anticyclonic eddies (C:A Ratio) is shown after normalization to total *Prochlorococcus* transcripts. *Corrected p-value < 0.05.
[a]Significantly regulated in *Prochlorococcus* MED4 and *Prochlorococcus* MIT9313, Thompson et al. (2011). [b]Shire and Kustka (2015).

these genes in the cyclonic eddy DCM, it seems possible that Fe stress only emerged in *Prochlorococcus* during long-term incubations.

Overall, this analysis suggests that the relatively high Fe requirements of *Prochlorococcus* under low irradiance may make them more sensitive to Fe limitation in the DCM than eukaryotic phytoplankton, even if *Prochlorococcus* was not Fe-limited outside of the multi-day incubations. It is interesting that this scenario is opposite to that outlined in the surface waters of the Equatorial Pacific, where *Prochlorococcus* tend to be less vulnerable to Fe limitation than eukaryotic phytoplankton (Cavender-Bares et al., 1999; Mann & Chisholm, 2000; Price et al., 1994). There, the small size of *Prochlorococcus* makes them more competitive for diffusive supply of recycled Fe, which may be largely unchelated (Morel et al., 2008). Bioassays and molecular studies have suggested that eukaryotic phytoplankton may be able to access a much larger portion of the dFe pool than *Prochlorococcus* (Coale et al., 2019; Kazamia et al., 2018; Lis et al., 2015; Maldonado & Price, 1999, 2001). Low irradiance near the DCM also makes Fe-chelates less prone to photodegradation or Fe photoreduction than tropical surface waters (Barbeau et al., 2001), likely increasing reliance on specific transport mechanisms rather than uptake systems based on inorganic Fe. In the on-deck incubations under DCM conditions, added Fe amphibactin D decreased markedly after 5 days in cyclonic eddy waters (Figure 7b), indicating that these compounds were bioavailable and that they cycle rapidly in the lower euphotic zone. It is interesting to note that similar removal was also apparent in the relatively Fe-rich anticyclone. Compared to the cyclone, the anticyclone DCM contained a similar number of heterotrophic bacteria but fewer picoeukaryotes and more *Prochlorococcus* (Figure 4), suggesting that the observed drawdown of siderophores may not depend on phytoplankton alone.

3.6. Implications for Iron Limitation in the Oligotrophic DCM

Taken together, these results highlight the potential for Fe stress within the microbial community in the cyclonic eddy center, which ultimately did not manifest in Fe limitation of primary production. It is noteworthy that dFe measured in the cyclonic eddy was almost identical to dFe in the lower euphotic zone at Station ALOHA (Table 1; Fitzsimmons et al., 2015). However, at similar irradiance, the cyclonic eddy supported a nearly two-fold increase in primary production relative to mean rates at Station ALOHA (Figure 5), which increased further in the long term incubations (Figure 6). Therefore, low dFe (50–80 pM) does not necessarily prevent increases in primary production under low light conditions.

Fe limitation of eukaryotic phytoplankton was recently reported for the DCM in the Eastern North Pacific (Hogle et al., 2018), especially close to the California coast where shoaling of isopycnal surfaces leads to greater NO_3^- supply to the lower euphotic zone (2.9–9.1 µM at the DCM), but similar dFe (0.05–0.1 nM). Other incubations at similarly high NO_3^-, but higher dFe (>0.2 nM), have shown signs of Fe-light co-limitation, but no response to Fe addition alone (Hopkinson & Barbeau, 2008; Johnson et al., 2010). From this perspective, it is likely that the cyclonic eddy did not reach a critical rate of N supply to trigger Fe limitation for the entire phytoplankton community. Relative to eddy lifetimes on the order of 100 days or more, the short-term nature of sampling and experiments may limit this conclusion to the mature phase of these eddies. Depending on the relative kinetics

of Fe and NO_3^- uptake following isopycnal uplift, more favorable conditions for Fe limitation (>1 μM NO_3^-, <0.1 nM dFe) may still emerge during cyclonic eddy intensification.

Compared to long term observations at Station ALOHA, however, the 2017 cyclonic and anticyclonic eddies were clearly anomalous, bracketing the extremes of sea-level anomaly and the displacement of isopycnal surfaces (Barone et al., Under Revision). The fact that isopycnal shoaling and enhanced NO_3^- supply in the 2017 cyclonic eddy was insufficient to induce Fe limitation of primary production means that the possibility for Fe limitation under non-eddy conditions should be relatively narrow. Similar conclusions are reached based on retrospective analyses of the HOT program (Barone et al., 2019; Church et al., 2009). Episodes of negative sea-surface height anomaly at Station ALOHA coincide with negative isopycnal NO_3^- anomalies in the lower euphotic zone and with positive anomalies in chlorophyll, productivity and oxygen (Table S1 in Supporting Information S1; Barone et al., 2019). These anomalies are best explained by processes also observed in the MESO-SCOPE cyclonic eddy center in July 2017: isopycnal uplift into the euphotic zone enables primary production and NO_3^- removal. The population of picoeukaryotes also increases during these events (Barone et al., 2019). Thus, eddy-driven NO_3^- drawdown in the lower euphotic zone has been observed on several instances, suggesting that the amount of dFe that is brought into the euphotic zone is sufficient for NO_3^- uptake. Anticyclonic eddies and other episodes of positive SLA_{corr} at Station ALOHA also support our observations from 2017: surface dFe injection into the lower euphotic zone following a depression of the thermocline does not lead to elevated productivity or O_2 concentration (Barone et al., 2019).

4. Conclusions

The pair of eddies sampled in the 2017 MESO-SCOPE project depict distinct NO_3^- and dFe supply regimes at the depths and isolumes that characterize the DCM (Figure 5, Table 1). In the cyclonic eddy, prior removal of NO_3^- and dFe, presumably during the intensification stage, was evident in isopycnal anomalies. Low $dFe:NO_3^-$ supply ratios from turbulent mixing also characterized the mature phase of the cyclone. The magnitude of these ratios are associated with Fe stress in *Prochlorococcus*, but may be sufficient for the picoeukaryote population found in this eddy. Compared to Station ALOHA, atypically high primary production near the 0.5 mol photon m^{-2} day^{-1} isolume in the cyclonic eddy was supported by elevated NO_3^- but similar dFe, implying that any regulating role for iron is secondary to nitrogen and light (Figure 5). Although unconfirmed by direct measurements, population control by grazers also appears to play a key role in recycling dFe to sustain this elevated productivity throughout the mature phase of these eddies. However, there are still key aspects of Fe budgets in the lower euphotic zone that are not constrained or considered by this work and likely influence the ecosystem susceptibility to iron stress, especially the magnitude and lability of particulate Fe inventories and the bioavailability of dFe. For now, we can only highlight the apparently rapid alterations of the siderophore pool as an indicator for a fast and complex iron cycle near the DCM (Figure 7).

Meanwhile, the unusual abundance of dFe in the anticyclone DCM should have created conditions to relieve Fe-stress. In some ways, this conceptual model is consistent with elevated *Prochlorococcus* abundance in the anticyclonic eddy, and with signs of Fe stress in leucine uptake experiments in the cyclone, but not the anticyclone. However, the fact that ^{14}C primary production profiles in the anticyclone overlapped with Station ALOHA mean values implies that any Fe fertilization effect must be small in magnitude or constrained by depletion of other nutrients (e.g., nitrogen). To the extent that the biogeochemistry documented within the MESO-SCOPE eddies and at Station ALOHA represent the North Pacific Subtropical Gyre and oligotrophic regions elsewhere, our results suggest that Fe limitation is difficult to induce in the DCM. However, given its apparently higher Fe requirements, one might look for *Prochlorococcus* in the DCM as a bellwether of Fe stress that would precede the emergence of Fe limitation at the ecosystem scale.

Conflict of Interest

The authors declare no conflicts of interest relevant to this study.

Data Availability Statement

Data from this manuscript can be accessed at https://doi.org/10.5281/zenodo.5064292 and https://doi.org/10.5281/zenodo.3750468. Amplicon sequence data can be accessed at the National Center for Biotechnology Information (NCBI) under sequence read archive PRJNA733670.

References

Achterberg, E. P., Moore, C. M., Henson, S. A., Steigenberger, S., Stohl, A., Eckhardt, S., et al. (2013). Natural iron fertilization by the Eyjafjallajökull volcanic eruption. *Geophysical Research Letters*, *40*(5), 921–926. https://doi.org/10.1002/grl.50221

Barbeau, K., Rue, E. L., Bruland, K. W., & Butler, A. (2001). Photochemical cycling of iron in the surface ocean mediated by microbial iron (III)-binding ligands. *Nature*, *413*(6854), 409–413. https://doi.org/10.1038/35096545

Barone, B., Coenen, A. R., Beckett, S. J., McGillicuddy, D. J., Weitz, J. S., & Karl, D. M. (2019). The ecological and biogeochemical state of the North Pacific Subtropical Gyre is linked to sea surface height. *Journal of Marine Research*, *77*(2), 215–245. https://doi.org/10.1357/002224019828474241

Becker, K. W., Harke, M. J., Mende, D. R., Muratore, D., Weitz, J. S., DeLong, E. F., et al. (2021). Combined pigment and metatranscriptomic analysis reveals highly synchronized diel patterns of phenotypic light response across domains in the open oligotrophic ocean. *The ISME Journal*, *15*(2), 520–533. https://doi.org/10.1038/s41396-020-00793-x

Berube, P. M., Coe, A., Roggensack, S. E., & Chisholm, S. W. (2016). Temporal dynamics of *Prochlorococcus* cells with the potential for nitrate assimilation in the subtropical Atlantic and Pacific oceans. *Limnology and Oceanography*, *61*(2), 482–495. https://doi.org/10.1002/lno.10226

Berube, P. M., Rasmussen, A., Braakman, R., Stepanauskas, R., & Chisholm, S. W. (2019). Emergence of trait variability through the lens of nitrogen assimilation in *Prochlorococcus*. *eLife*, *8*, e41043. https://doi.org/10.7554/elife.41043

Bibby, T. S., Mary, I., Nield, J., Partensky, F., & Barber, J. (2003). Low-light-adapted *Prochlorococcus* species possess specific antennae for each photosystem. *Nature*, *424*(6952), 1051–1054. https://doi.org/10.1038/nature01933

Bishop, J. K. B., Davis, R. E., & Sherman, J. T. (2002). Robotic observations of dust storm enhancement of carbon biomass in the North Pacific. *Science*, *298*(5594), 817–821. https://doi.org/10.1126/science.1074961

Björkman, K. M., Church, M. J., Doggett, J. K., & Karl, D. M. (2015). Differential assimilation of inorganic carbon and leucine by *Prochlorococcus* in the oligotrophic North Pacific subtropical gyre. *Frontiers in Microbiology*, *6*, 1401.

Blain, S., Quéguiner, B., Armand, L., Belviso, S., Bombled, B., Bopp, L., et al. (2007). Effect of natural iron fertilization on carbon sequestration in the Southern Ocean. *Nature*, *446*(7139), 1070–1074. https://doi.org/10.1038/nature05700

Boiteau, R. M., Mende, D. R., Hawco, N. J., McIlvin, M. R., Fitzsimmons, J. N., Saito, M. A., et al. (2016). Siderophore-based microbial adaptations to iron scarcity across the eastern Pacific Ocean. *Proceedings of the National Academy of Sciences of the United States of America*, *113*(50), 14237–14242. https://doi.org/10.1073/pnas.1608594113

Boiteau, R. M., & Repeta, D. J. (2015). An extended siderophore suite from *Synechococcus* sp. PCC 7002 revealed by LC-ICPMS-ESIMS. *Metallomics*, *7*(5), 877–884. https://doi.org/10.1039/c5mt00005j

Boyd, P. W., Jickells, T., Law, C. S., Blain, S., Boyle, E. A., Buesseler, K. O., et al. (2007). Mesoscale iron enrichment experiments 1993-2005: Synthesis and future directions. *Science*, *315*(5812), 612–617. https://doi.org/10.1126/science.1131669

Boyle, E. A., Bergquist, B. A., Kayser, R. A., & Mahowald, N. (2005). Iron, manganese, and lead at Hawaii Ocean Time-series station ALOHA: Temporal variability and an intermediate water hydrothermal plume. *Geochimica et Cosmochimica Acta*, *69*(4), 933–952. https://doi.org/10.1016/j.gca.2004.07.034

Browning, T. J., Al-Hashem, A. A., Hopwood, M. J., Engel, A., Belkin, I. M., Wakefield, E. D., et al. (2021). Iron regulation of North Atlantic eddy phytoplankton productivity. *Geophysical Research Letters*, *48*, e2020GL091403. https://doi.org/10.1029/2020gl091403

Bruland, K. W., Orians, K. J., & Cowen, J. P. (1994). Reactive trace metals in the stratified central North Pacific. *Geochimica et Cosmochimica Acta*, *58*(15), 3171–3182. https://doi.org/10.1016/0016-7037(94)90044-2

Bundy, R. M., Boiteau, R. M., McLean, C., Turk-Kubo, K. A., McIlvin, M. R., Saito, M. A., et al. (2018). Distinct siderophores contribute to iron cycling in the mesopelagic at station ALOHA. *Frontiers in Marine Science*, *5*, 61. https://doi.org/10.3389/fmars.2018.00061

Callahan, B. J., McMurdie, P. J., Rosen, M. J., Han, A. W., Johnson, A. J. A., & Holmes, S. P. (2016). DADA2: High-resolution sample inference from Illumina amplicon data. *Nature Methods*, *13*, 581–583. https://doi.org/10.1038/nmeth.3869

Casey, J. R., Lomas, M. W., Mandecki, J., & Walker, D. E. (2007). *Prochlorococcus* contributes to new production in the Sargasso Sea deep chlorophyll maximum. *Geophysical Research Letters*, *34*(10), L10604. https://doi.org/10.1029/2006gl028725

Cavender-Bares, K. K., Mann, E. L., Chisholm, S. W., Ondrusek, M. E., & Bidigare, R. R. (1999). Differential response of equatorial Pacific phytoplankton to iron fertilization. *Limnology and Oceanography*, *44*(2), 237–246. https://doi.org/10.4319/lo.1999.44.2.0237

Chelton, D. B., Schlax, M. G., & Samelson, R. M. (2011). Global observations of nonlinear mesoscale eddies. *Progress in Oceanography*, *91*(2), 167–216. https://doi.org/10.1016/j.pocean.2011.01.002

Church, M. J., Ducklow, H. W., Letelier, R. M., & Karl, D. M. (2006). Temporal and vertical dynamics in picoplankton photoheterotrophic production in the subtropical North Pacific Ocean. *Aquatic Microbial Ecology*, *45*(1), 41–53. https://doi.org/10.3354/ame045041

Church, M. J., Mahaffey, C., Letelier, R. M., Lukas, R., Zehr, J. P., & Karl, D. M. (2009). Physical forcing of nitrogen fixation and diazotroph community structure in the North Pacific subtropical gyre. *Global Biogeochemical Cycles*, *23*(2), GB2020. https://doi.org/10.1029/2008GB003418

Coale, K. H., Fitzwater, S. E., Gordon, R. M., Johnson, K. S., & Barber, R. T. (1996). Control of community growth and export production by upwelled iron in the equatorial Pacific Ocean Kenneth. *Nature*, *379*, 621–624. https://doi.org/10.1038/379621a0

Coale, T. H., Moosburner, M., Horák, A., Oborník, M., Barbeau, K. A., & Allen, A. E. (2019). Reduction-dependent siderophore assimilation in a model pennate diatom. *Proceedings of the National Academy of Sciences of the United States of America*, *116*(47), 23609–23617. https://doi.org/10.1073/pnas.1907234116

Cullen, J. J. (2015). Subsurface chlorophyll maximum layers: Enduring enigma or mystery solved? *Annual Review of Marine Science*, *7*, 207–239. https://doi.org/10.1146/annurev-marine-010213-135111

Cunningham, B. R., & John, S. G. (2017). The effect of iron limitation on cyanobacteria major nutrient and trace element stoichiometry. *Limnology and Oceanography*, *62*(2), 846–858. https://doi.org/10.1002/lno.10484

Duhamel, S., Van Wambeke, F., Lefevre, D., Benavides, M., & Bonnet, S. (2018). Mixotrophic metabolism by natural communities of unicellular cyanobacteria in the western tropical South Pacific Ocean. *Environmental Microbiology*, *20*(8), 2743–2756. https://doi.org/10.1111/1462-2920.14111

Ellwood, M. J., Strzepek, R. F., Strutton, P. G., Trull, T. W., Fourquez, M., & Boyd, P. W. (2020). Distinct iron cycling in a Southern Ocean eddy. *Nature Communications*, *11*(1), 1–8. https://doi.org/10.1038/s41467-020-14464-0

Fitzsimmons, J. N., Hayes, C. T., Al-Subiai, S. N., Zhang, R., Morton, P. L., Weisend, R. E., et al. (2015). Daily to decadal variability of size-fractionated iron and iron-binding ligands at the Hawaii Ocean Time-series Station ALOHA. *Geochimica et Cosmochimica Acta*, *171*, 303–324. https://doi.org/10.1016/j.gca.2015.08.012

Foreman, R. K., Segura-Noguera, M., & Karl, D. M. (2016). Validation of Ti (III) as a reducing agent in the chemiluminescent determination of nitrate and nitrite in seawater. *Marine Chemistry*, *186*, 83–89. https://doi.org/10.1016/j.marchem.2016.08.003

Gifford, S. M., Becker, J. W., Sosa, O. A., Repeta, D. J., & DeLong, E. F. (2016). Quantitative transcriptomics reveals the growth-and nutrient-dependent response of a streamlined marine methylotroph to methanol and naturally occurring dissolved organic matter. *MBio*, *7*(6). https://doi.org/10.1128/mbio.01279-16

Hamme, R. C., Webley, P. W., Crawford, W. R., Whitney, F. A., DeGrandpre, M. D., Emerson, S. R., et al. (2010). Volcanic ash fuels anomalous plankton bloom in subarctic northeast Pacific. *Geophysical Research Letters*, *37*(19), L19604. https://doi.org/10.1029/2010gl044629

Hawco, N. J., Fu, F., Yang, N., Hutchins, D. A., & John, S. G. (2021). Independent iron and light limitation in a low-light-adapted *Prochlorococcus* from the deep chlorophyll maximum. *The ISME Journal*, *15*(1), 359–362. https://doi.org/10.1038/s41396-020-00776-y

Hawco, N. J., Yang, S.-C., Foreman, R. K., Funkey, C. P., Dugenne, M., White, A. E., et al. (2020). Metal isotope signatures from lava-seawater interaction during the 2018 eruption of Kīlauea. *Geochimica et Cosmochimica Acta*, *282*, 340–356. https://doi.org/10.1016/j.gca.2020.05.005

Hogle, S. L., Dupont, C. L., Hopkinson, B. M., King, A. L., Buck, K. N., Roe, K. L., et al. (2018). Pervasive iron limitation at subsurface chlorophyll maxima of the California Current. *Proceedings of the National Academy of Sciences of the United States of America*, *115*(52), 13300–13305. https://doi.org/10.1073/pnas.1813192115

Hopkinson, B. M., & Barbeau, K. A. (2008). Interactive influences of iron and light limitation on phytoplankton at subsurface chlorophyll maxima in the eastern North Pacific. *Limnology and Oceanography*, *53*(4), 1303–1318. https://doi.org/10.4319/lo.2008.53.4.1303

Johnson, Z. I., Shyam, R., Ritchie, A. E., Mioni, C., Lance, V. P., Murray, J. W., & Zinser, E. R. (2010). The effect of iron-and light-limitation on phytoplankton communities of deep chlorophyll maxima of the western Pacific Ocean. *Journal of Marine Research*, *68*(2), 283–308. https://doi.org/10.1357/002224010793721433

Karl, D. M., Letelier, R. M., Bidigare, R. R., Björkman, K. M., Church, M. J., Dore, J. E., & White, A. E. (2021). Seasonal-to-decadal scale variability in primary production and particulate matter export at Station ALOHA. *Progress in Oceanography*, *195*, 102563. https://doi.org/10.1016/j.pocean.2021.102563

Kazamia, E., Sutak, R., Paz-Yepes, J., Dorrell, R. G., Vieira, F. R. J., Mach, J., et al. (2018). Endocytosis-mediated siderophore uptake as a strategy for Fe acquisition in diatoms. *Science Advances*, *4*(5), eaar4536. https://doi.org/10.1126/sciadv.aar4536

Letelier, R. M., Bidigare, R. R., Hebel, D. V., Ondrusek, M., Winn, C. D., & Karl, D. M. (1993). Temporal variability of phytoplankton community structure based on pigment analysis. *Limnology and Oceanography*, *38*(7), 1420–1437. https://doi.org/10.4319/lo.1993.38.7.1420

Letelier, R. M., Karl, D. M., Abbott, M. R., & Bidigare, R. R. (2004). Light driven seasonal patterns of chlorophyll and nitrate in the lower euphotic zone of the North Pacific Subtropical Gyre. *Limnology and Oceanography*, *49*(2), 508–519. https://doi.org/10.4319/lo.2004.49.2.0508

Lis, H., Shaked, Y., Kranzler, C., Keren, N., & Morel, F. M. M. (2015). Iron bioavailability to phytoplankton: An empirical approach. *The ISME Journal*, *9*(4), 1003–1013. https://doi.org/10.1038/ismej.2014.199

Lorenzen, C. J. (1967). Determination of chlorophyll and pheo-pigments: Spectrophotometric equations 1. *Limnology and Oceanography*, *12*(2), 343–346. https://doi.org/10.4319/lo.1967.12.2.0343

Maldonado, M. T., & Price, N. M. (1996). Influence of N substrate on Fe requirements of marine centric diatoms. *Marine Ecology Progress Series*, *141*, 161–172. https://doi.org/10.3354/meps141161

Maldonado, M. T., & Price, N. M. (1999). Utilization of iron bound to strong organic ligands by plankton communities in the subarctic Pacific Ocean. *Deep Sea Research Part II: Topical Studies in Oceanography*, *46*(11–12), 2447–2473. https://doi.org/10.1016/s0967-0645(99)00071-5

Maldonado, M. T., & Price, N. M. (2001). Reduction and transport of organically bound iron by *Thalassiosira oceanica* (Bacillariophyceae). *Journal of Phycology*, *37*(2), 298–310. https://doi.org/10.1046/j.1529-8817.2001.037002298.x

Malmstrom, R. R., Coe, A., Kettler, G. C., Martiny, A. C., Frias-Lopez, J., Zinser, E. R., & Chisholm, S. W. (2010). Temporal dynamics of *Prochlorococcus* ecotypes in the Atlantic and Pacific oceans. *The ISME Journal*, *4*(10), 1252–1264. https://doi.org/10.1038/ismej.2010.60

Mann, E. L., & Chisholm, S. W. (2000). Iron limits the cell division rate of *Prochlorococcus* in the eastern equatorial Pacific. *Limnology and Oceanography*, *45*(5), 1067–1076. https://doi.org/10.4319/lo.2000.45.5.1067

Marchetti, A., Maldonado, M. T., Lane, E. S., & Harrison, P. J. (2006). Iron requirements of the pennate diatom *Pseudo-nitzschia*: Comparison of oceanic (high-nitrate, low-chlorophyll waters) and coastal species. *Limnology and Oceanography*, *51*(5), 2092–2101. https://doi.org/10.4319/lo.2006.51.5.2092

Martin, J. H., Coale, K. H., Johnson, K. S., Fitzwater, S. E., Gordon, R. M., Tanner, S. J., et al. (1994). Testing the iron hypothesis in ecosystems of the equatorial Pacific Ocean. *Nature*, *371*, 123–129. https://doi.org/10.1038/371123a0

Martin, J. H., Gordon, R. M., & Fitzwater, S. E. (1990). Iron in Antarctic waters. *Nature*, *345*(6271), 156–158. https://doi.org/10.1038/345156a0

McGillicuddy, D. J., Jr. (2016). Mechanisms of physical-biological-biogeochemical interaction at the oceanic mesoscale. *Annual Review of Marine Science*. 8, 125–159. https://doi.org/10.1146/annurev-marine-010814-015606

Mignot, A., Claustre, H., Uitz, J., Poteau, A., d'Ortenzio, F., & Xing, X. (2014). Understanding the seasonal dynamics of phytoplankton biomass and the deep chlorophyll maximum in oligotrophic environments: A Bio-Argo float investigation. *Global Biogeochemical Cycles*, *28*(8), 856–876. https://doi.org/10.1002/2013gb004781

Moore, C. M., Mills, M. M., Arrigo, K. R., Berman-Frank, I., Bopp, L., Boyd, P. W., et al. (2013). Processes and patterns of oceanic nutrient limitation. *Nature Geoscience*, *6*(9), 701–710. https://doi.org/10.1038/ngeo1765

Moore, J. K., Doney, S. C., Glover, D. M., & Fung, I. Y. (2001). Iron cycling and nutrient-limitation patterns in surface waters of the World Ocean. *Deep Sea Research Part II: Topical Studies in Oceanography*, *49*(1–3), 463–507. https://doi.org/10.1016/s0967-0645(01)00109-6

Moore, L. R., Post, A. F., Rocap, G., & Chisholm, S. W. (2002). Utilization of different nitrogen sources by the marine cyanobacteria *Prochlorococcus* and *Synechococcus*. *Limnology and Oceanography*, *47*(4), 989–996. https://doi.org/10.4319/lo.2002.47.4.0989

Morel, F. M. M., Hudson, R. J. M., & Price, N. M. (1991). Limitation of productivity by trace metals in the sea. *Limnology and Oceanography*, *36*(8), 1742–1755. https://doi.org/10.4319/lo.1991.36.8.1742

Morel, F. M. M., Kustka, A. B., & Shaked, Y. (2008). The role of unchelated Fe in the iron nutrition of phytoplankton. *Limnology and Oceanography*, *53*(1), 400–404. https://doi.org/10.4319/lo.2008.53.1.0400

Pollard, R. T., Salter, I., Sanders, R. J., Lucas, M. I., Moore, C. M., Mills, R. A., et al. (2009). Southern Ocean deep-water carbon export enhanced by natural iron fertilization. *Nature*, *457*(7229), 577–580. https://doi.org/10.1038/nature07716

Price, N. M., Ahner, B. A., & Morel, F. M. M. (1994). The equatorial Pacific Ocean: Grazer-controlled phytoplankton populations in an iron-limited ecosystem 1. *Limnology and Oceanography*, *39*(3), 520–534. https://doi.org/10.4319/lo.1994.39.3.0520

Raven, J. A. (1988). The iron and molybdenum use efficiencies of plant growth with different energy, carbon and nitrogen sources. *New Phytologist*, *109*(3), 279–287. https://doi.org/10.1111/j.1469-8137.1988.tb04196.x

Raven, J. A. (1990). Predictions of Mn and Fe use efficiencies of phototrophic growth as a function of light availability for growth and of C assimilation pathway. *New Phytologist*, *116*(1), 1–18. https://doi.org/10.1111/j.1469-8137.1990.tb00505.x

Rii, Y. M., Karl, D. M., & Church, M. J. (2016). Temporal and vertical variability in picophytoplankton primary productivity in the North Pacific Subtropical Gyre. *Marine Ecology Progress Series*, *562*, 1–18. https://doi.org/10.3354/meps11954

Sedwick, P. N., Bowie, A. R., Church, T. M., Cullen, J. T., Johnson, R. J., Lohan, M. C., et al. (2020). Dissolved iron in the Bermuda region of the subtropical North Atlantic Ocean: Seasonal dynamics, mesoscale variability, and physicochemical speciation. *Marine Chemistry*, *219*, 103748. https://doi.org/10.1016/j.marchem.2019.103748

Sedwick, P. N., Church, T. M., Bowie, A. R., Marsay, C. M., Ussher, S. J., Achilles, K. M., et al. (2005). Iron in the Sargasso Sea (Bermuda Atlantic Time-series Study region) during summer: Eolian imprint, spatiotemporal variability, and ecological implications. *Global Biogeochemical Cycles*, *19*(4), GB4006. https://doi.org/10.1029/2004gb002445

Shire, D. M., & Kustka, A. B. (2015). Luxury uptake, iron storage and ferritin abundance in *Prochlorococcus* marinus (Synechococcales) strain MED4. *Phycologia*, *54*(4), 398–406. https://doi.org/10.2216/14-109.1

Siegel, D. A., McGillicuddy, D. J., Jr, & Fields, E. A. (1999). Mesoscale eddies, satellite altimetry, and new production in the Sargasso Sea. *Journal of Geophysical Research*, *104*(C6), 13359–13379. https://doi.org/10.1029/1999jc900051

Strickland, J. D. H., & Parsons, T. R. (1972). *A practical handbook of seawater analysis*.

Strong, A., Chisholm, S., Miller, C., & Cullen, J. (2009). Ocean fertilization: Time to move on. *Nature*, *461*(7262), 347–348. https://doi.org/10.1038/461347a

Strzepek, R. F., Boyd, P. W., & Sunda, W. G. (2019). Photosynthetic adaptation to low iron, light, and temperature in Southern Ocean phytoplankton. *Proceedings of the National Academy of Sciences of the United States of America*, *116*(10), 4388–4393. https://doi.org/10.1073/pnas.1810886116

Strzepek, R. F., Hunter, K. A., Frew, R. D., Harrison, P. J., & Boyd, P. W. (2012). Iron-light interactions differ in Southern Ocean phytoplankton. *Limnology and Oceanography*, *57*(4), 1182–1200. https://doi.org/10.4319/lo.2012.57.4.1182

Sunda, W., Price, N., Morel, F., Service, N. O., & Road, P. I. (2005). Trace metal ion buffers and their use in culture studies. In *Algal culturing techniques* (pp. 35–63). Academic Press. https://doi.org/10.1016/b978-012088426-1/50005-6

Sunda, W. G., & Huntsman, S. A. (1997). Interrelated influence of iron, light and cell size on marine phytoplankton growth. *Nature*, *390*(6658), 389–392. https://doi.org/10.1038/37093

Thompson, A. W., Huang, K., Saito, M. A., & Chisholm, S. W. (2011). Transcriptome response of high- and low-light-adapted *Prochlorococcus* strains to changing iron availability. *The ISME Journal*, *5*, 1580–1594. https://doi.org/10.1038/ismej.2011.49

Virtanen, P., Gommers, R., Oliphant, T. E., Haberland, M., Reddy, T., Cournapeau, D., et al. (2020). SciPy 1.0: Fundamental algorithms for scientific computing in Python. *Nature Methods*, *17*(3), 261–272. https://doi.org/10.1038/s41592-020-0772-5

Viviani, D. A., & Church, M. J. (2017). Decoupling between bacterial production and primary production over multiple time scales in the North Pacific Subtropical Gyre. *Deep Sea Research Part I: Oceanographic Research Papers*, *121*, 132–142. https://doi.org/10.1016/j.dsr.2017.01.006

Ward, B. A., Dutkiewicz, S., Moore, C. M., & Follows, M. J. (2013). Iron, phosphorus, and nitrogen supply ratios define the biogeography of nitrogen fixation. *Limnology and Oceanography*, *58*(6), 2059–2075. https://doi.org/10.4319/lo.2013.58.6.2059

Wilson, S. T., Aylward, F. O., Ribalet, F., Barone, B., Casey, J. R., Connell, P. E., et al. (2017). Coordinated regulation of growth, activity and transcription in natural populations of the unicellular nitrogen-fixing cyanobacterium *Crocosphaera*. *Nature Microbiology*, *2*(9), 1–9. https://doi.org/10.1038/nmicrobiol.2017.118

Wilson, S. T., Hawco, N. J., Armbrust, E. V., Barone, B., Björkman, K. M., Boysen, A. K., et al. (2019). Kīlauea lava fuels phytoplankton bloom in the North Pacific Ocean. *Science*, *365*(6457), 1040–1044. https://doi.org/10.1126/science.aax4767

Wu, J., Sunda, W., Boyle, E. A., & Karl, D. M. (2000). Phosphate depletion in the western North Atlantic Ocean. *Science*, *289*(5480), 759–762. https://doi.org/10.1126/science.289.5480.759

Wunsch, C. (1997). The vertical partition of oceanic horizontal kinetic energy. *Journal of Physical Oceanography*, *27*(8), 1770–1794. https://doi.org/10.1175/1520-0485(1997)027<1770:tvpooh>2.0.co;2

Zhang, Z., Wang, W., & Qiu, B. (2014). Oceanic mass transport by mesoscale eddies. *Science*, *345*(6194), 322–324. https://doi.org/10.1126/science.1252418